Synthesis and Microstructural Characterisation of Two New One-Dimensional Members of the $(A_3NiMnO_6)_\alpha(A_3Mn_3O_9)_\beta$ Homologous Series (A = Ba, Sr)

María Hernando,[a] Khalid Boulahya,[a] Marina Parras,[a] Jose M. González-Calbet,*[a] and Ulises Amador[b]

Keywords: Electron diffraction / High-resolution electron microscopy / One-dimensional oxides / Twinned microstructure

Two new members of the one-dimensional $(A_3NiMnO_6)_\alpha(A_3Mn_3O_9)_\beta$ homologous series, with the compositions $(Sr_{0.75}Ba_{0.25})_5NiMn_3O_{12}$ and $Sr_9Ni_2Mn_5O_{21}$, have been synthesised. Their structures can each be described as a hexagonal array of infinite one-dimensional chains of face-sharing polyhedra, running parallel to the *c* axis and separated by the Sr/Ba cations. The structure of $(Sr_{0.75}Ba_{0.25})_5NiMn_3O_{12}$, which constitutes the ($\alpha = 3$, $\beta = 2$) member of the series, is made up of three face-sharing octahedra linked by one trigonal prism. For $Sr_9Ni_2Mn_5O_{21}$ ($\alpha = 2$, $\beta = 1$) the sequence of polyhedra along the chains corresponds to a motif consisting of two octahedra–one trigonal prism–three octahedra–one trigonal prism. The manganese atoms occupy the octahedral sites in both phases, while the Ni^{2+} cations are distributed in the trigonal-prismatic sites in a disordered way. Only a small fraction of these (close to 20%) is located at the centres of the trigonal prisms, 80% being displaced towards the rectangular faces of the polyhedra and giving rise to a square-planar-like coordination. Both oxides present twinned microstructures, as evidenced by SAED and HREM.

Introduction

Growing interest has recently developed in a family of materials structurally related both to $A_3A'BO_6$ (K_4CdCl_6-type)[1] and to 2H-ABO_3 hexagonal perovskite.[2] In the former oxide, $A'O_6$ trigonal prisms (TP) and BO_6 octahedra (Oh) share triangular faces, in a 1:1 sequence, forming infinite polyhedra chains parallel to the *c* axis of a rhombohedral unit cell. The 2H-ABO_3 hexagonal perovskite is also composed of a hexagonal array of infinite chains, but the chains in this case are made up of face-sharing BO_6 octahedra. A large number of intermediate structures obtained by varying the number of octahedra between the trigonal prisms, maintaining the hexagonal array of the polyhedra one-dimensional chains have been described. In fact, all of these can be regarded as being formed by the ordered intergrowth of the structural units constituting the above structures. This building principle gives rise to the $(A_3A'BO_6)_\alpha(A_3B_3O_9)_\beta$ general formula, in which α and β denote the number of $A_3A'BO_6$ and 2H-ABO_3 structural blocks, respectively, in each term.[3]

A large number of oxides belonging to this family have been reported, due in part to the variety of elements that can be introduced into the oxygen framework. In this sense, the A cation usually corresponds to an alkaline earth metal, whilst the A′ and B sites can be occupied by many different metal atoms. In addition, the A′ and the B positions can be occupied by the same cation. Much of the work published on these materials has been performed on the A−(A′ = B)−O systems, in which A′ = B = Ni,[4,5] Co[6−8] and A = Ba, Sr, Ca. In the different stabilized members, Ni or Co seem to present both II and IV oxidation states.

When A′ = B = Mn, no one-dimensional hexagonal phases are known. In this sense it is worth noting that two-dimensional phases, also structurally related to 2H-$BaMnO_3$, have recently been reported. As an example, the compound $Ba_6Mn_5O_{16}$ [9] crystallizes in a laminar structure closely related to the 15-R polytype.[10] Note that Mn is only in the IV oxidation state. The same cationic relationship presents the one-dimensional $Ba_6Ni_5O_{15}$,[4] the ($\alpha = 3$, $\beta = 3$) member of the series, but Ni is now present both as Ni^{II} and as Ni^{IV}. According to this, one might think that one-dimensional oxides containing Mn as the sole metal in the polyhedra chains should be less stable, due to the low stability of Mn^{II} in a trigonal prism or in an octahedral environment. However, when A′ ≠ B = Mn, several one-dimensional phases in which Mn occupies the octahedral sites have been reported, whilst a metal of a different chemical nature, such as Zn,[11,12] Cu[13] or Ni,[14,16] is located in the TP. In the case of Ni, two phases have previously been reported: $Ca_3(Ni)_{TP}(Mn)_{Oh}O_6$ [14,15] and $Sr_4(Ni)_{TP}(Mn_2)_{Oh}O_9$,[16,17] corresponding to the ($\alpha = 3$, $\beta = 0$) and

[a] Departamento de Química Inorgánica, Facultad de Químicas, Universidad Complutense,
28040 Madrid, Spain
E-mail: jgcalbet@quim.ucm.es
[b] Departamento de Química, Facultad de Ciencias Experimentales y de la Salud, Universidad San Pablo-CEU,
28668 Madrid, Spain

($\alpha = 3$, $\beta = 1$) members of the series, respectively. In the former oxide, the polyhedra chains are made up of one octahedron and one trigonal prism sharing faces; in the latter, dimers of face-sharing octahedra are separated by one trigonal prism. In both cases, Mn ions, in the IV oxidation state, occupy the octahedral sites and Ni^{II} is situated in the TP positions. At this point it should be remarked that in some cases, such as in Ca_3NiMnO_6, the Ni atoms are located at the centres of the prisms, whereas in other cases, in $Sr_4Mn_2NiO_9$ for instance, approximately 80% of the Ni^{2+} ions are displaced towards one of the rectangular faces of the TP. This is fairly normal in Ni- or Cu-containing oxides such as Sr_3CuPtO_6,[18] $Sr_4Ni_3O_9$ [4] or $Sr_4CuIr_2O_9$.[19]

This paper reports the structural study of two new members, ($\alpha = 3$, $\beta = 2$) and ($\alpha = 2$, $\beta = 1$), of the $(A_3NiMnO_6)_\alpha(A_3Mn_3O_9)_\beta$ (A = Ba, Sr) series.

Results and Discussion

Chemical and Structural Characterization

Samples of nominal compositions $(Sr_{0.75}Ba_{0.25})_5NiMn_3O_{12}$ and $Sr_9Ni_2Mn_5O_{21}$ were confirmed to be single phases by X-ray diffraction (Figure 1). The average cationic ratios, determined by ICP, agree with the nominal compositions within experimental accuracy, the following metal

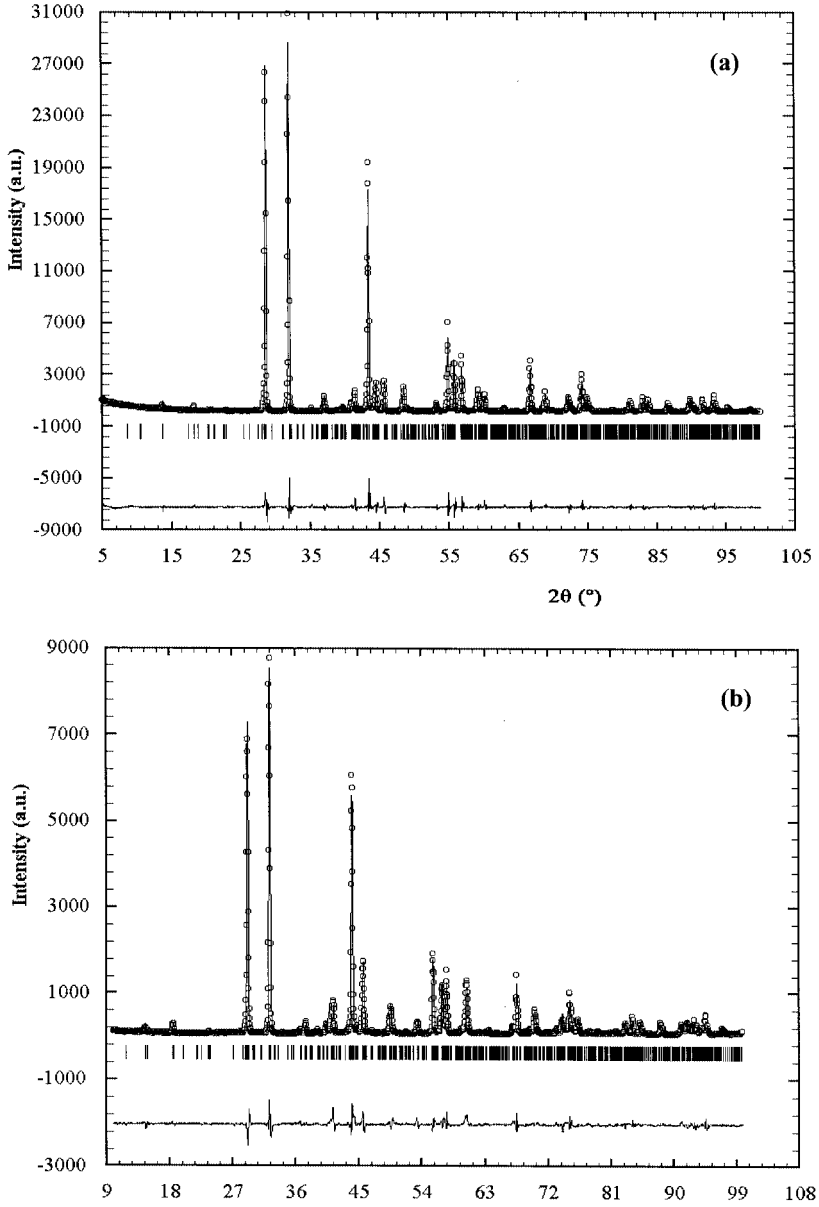

Figure 1. (a) Graphic results for the fitting of the X-ray powder diffraction data of $(Sr_{0.75}Ba_{0.25})_5NiMn_3O_{12}$: experimentally ascertained (points), calculated (solid line) and difference (bottom); (b) graphic results for the fitting of the X-ray powder diffraction data of $Sr_9Ni_2Mn_5O_{21}$: experimentally ascertained (points), calculated (solid line) and difference (bottom)

contents being obtained: Sr 35.88±0.9% (35.8%), Ba 17.7±0.4% (18.7%), Mn 17.8±0.4% (17.99%) and Ni 7.0±0.2% (6.5%) − in agreement with the nominal $Sr_{3.75}Ba_{1.25}NiMn_3O_{12}$ composition − and Sr 50.8±1.3% (51.99%), Mn 17.4±0.4% (18.1%) and Ni 7.84±0.2% (7.7%) − consistent with the $Sr_9Ni_2Mn_5O_{21}$ nominal composition. EDS analyses, performed on numerous crystallites with use of $SrMnO_3$ and $BaMnO_3$ as standards, confirm the above compositions.

Figure 1 (a) shows the X-ray diffraction pattern of $Sr_{3.75}Ba_{1.25}NiMn_3O_{12}$. The whole pattern can be indexed within a hexagonal unit cell of parameters $a = 0.97114(2)$ nm and $c = 2.03649(6)$ nm as corresponding to the ($\alpha = 3$, $\beta = 2$) member of the $(A_3A'BO_6)_\alpha(A_3B_3O_9)_\beta$ series. On the other hand, the corresponding XRD pattern of $Sr_9Ni_2Mn_5O_{21}$ is depicted in Figure 1 (b), all the peaks being indexed in a rhombohedral unit cell with $a = 0.96065(5)$ nm and $c = 3.5836(2)$ nm, in agreement with the structural characteristics of the ($\alpha = 2$, $\beta = 1$) term of the above one-dimensional family.

SAED and HREM

$(Sr_{0.75}Ba_{0.25})_5NiMn_3O_{12}$ ($\alpha = 3$, $\beta = 2$)

Microstructural characterization by SAED and HREM confirms the XRD results; the most relevant SAED patterns are shown in Figure 2 (a and b). All the maxima can be indexed in the hexagonal unit cell described above. The condition reflections are compatible with the $P\bar{3}c1$ space group previously proposed for isostructural $Sr_5Co_4O_{12}$.[7] In addition, the intensity distribution of the spots on the SAED pattern of Figure 2 (b) seems to indicate the presence of twinning in the crystals. Actually, Figure 2 (c) shows the same [1$\bar{2}$10] reciprocal plane corresponding to the untwinned isostructural oxide $Sr_5Co_4O_{12}$.[6] The intensity distribution of the spots corresponding to the (*h*0*i*2*h*) reflections is modulated. This feature is a general one in all one-dimensional oxides belonging to the $(A_3A'BO_6)_\alpha(A_3B_3O_9)_\beta$ series, the direction of the modulation always being perpendicular to the planes containing the metal atoms in the TP sites. When this SAED pattern is compared to that shown in Figure 2 (b), it can be observed that the modulated distribution of the intensity of the spots is apparent not only along the [*h*0*i*2*h*]* direction but also along the [$\bar{h}$0*i*2*h*]* direction. This is due to twinning of the crystals, as confirmed by HREM. Indeed, in the image taken along the [1$\bar{2}$10] zone axis, shown in Figure 3, two large identical domains, inclined towards one another around the *c* axis, are clearly observed. In both domains, *d* spacings of 0.83 and 1.01 nm − along the *c* and the *a* axes, respectively − are observed, such interplanar distances corresponding to d_{001} and d_{100} of the hexagonal unit cell described above. The contrast variation observed in both domains is characteristic of the $\alpha = 3$, $\beta = 2$ structure. In the magnification of one domain (Figure 3, b), it can be seen that, along the *c* axis, two bright dots alternate with three less intense dots. Such contrast variation can be attributed to the (Oh−Oh−Oh−TP) polyhedra sequence since, in all these one-dimensional oxides, the metal columns in the trigonal sites and the Sr/Ba atoms are imaged as bright dots. The calculated image (inset in Figure 3, b) agrees with the experimentally ascertained one for $\Delta t = 7.5$ and $\Delta f = -90$ nm.

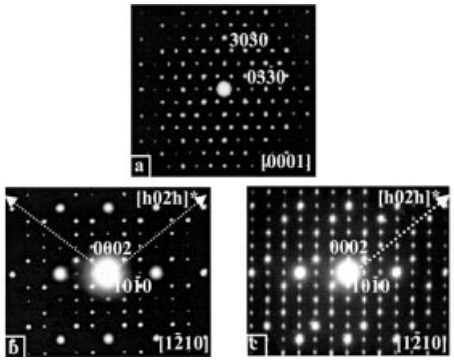

Figure 2. SAED patterns along the [0001] (a) and [1$\bar{2}$10] (b) zone axis corresponding to $(Sr_{0.75}Ba_{0.25})_5NiMn_3O_{12}$; (c) SAED pattern along the [1$\bar{2}$10] zone axis corresponding to $Sr_5Co_4O_{12}$

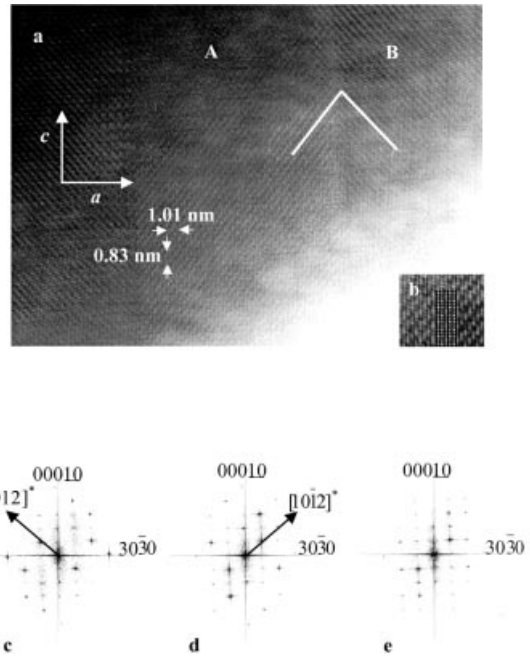

Figure 3. (a) HREM of $(Sr_{0.75}Ba_{0.25})_5NiMn_3O_{12}$ along [1$\bar{2}$10]; a twinned microstructure can clearly be seen; (b) magnification of one of the microdomains; calculated image is shown in the inset; optical Fourier transforms (FT) corresponding to domains marked with A (c) and B (d) in Figure 3a; (e) FT corresponding to the juxtaposition of both A and B domains

Optical Fourier Transforms of both domains, labelled A and B in Figure 3, are depicted in Figure 3 (c and d). Both patterns correspond to [1$\bar{2}$10]-oriented domains related to one another through a 90° rotation around *c**. Consequently, in the first domain, the intensity modulation is observed along the [*h*0*i*2*h*]* reciprocal direction whilst in the second domain the modulation is along the [$\bar{h}$0*i*2*h*]* one.

Juxtaposition of the two patterns (Figure 3, e) fits with the experimental one of Figure 2 (b).

$Sr_9Ni_2Mn_5O_{21}$ ($\alpha = 2$, $\beta = 1$)

Figure 4 (a) corresponds to the SAED pattern of the title sample along the [1$\bar{2}$10] zone axis. Once again, the features of this SAED suggest the presence of twinning in the crystal. Actually, Figure 4 (b) shows a typical [1$\bar{2}$10] reciprocal plane of an untwinned crystal of $(Sr_{0.6}Ca_{0.4})_9Co_7O_{21}$,[3] an ($\alpha = 2$, $\beta = 1$) term of the $(A_3A'BO_6)_\alpha(A_3B_3O_9)_\beta$ homologous series. Only the *hkl* reflections with $-h + k + l = 3n$ are observed, according to the rhombohedral symmetry of this phase (space group *R*3*c*). Note that the intensity distribution of the (*h*0*i*4*h*)* peaks is modulated in a similar way as in $(Sr_{0.75}Ba_{0.25})_5NiMn_3O_{12}$. Comparison between the SAED patterns shown in Figure 4 (a and b) highlights the presence of reflections forbidden for a rhombohedral symmetry in the pattern corresponding to $Sr_9Ni_2Mn_5O_{21}$. Moreover, the ($\bar{h}$0*i*4*h*) peaks are also present, and so a pseudo-trigonal symmetry results. This can be associated with the presence of twinning in the crystals, as confirmed by HREM. Actually, in the corresponding micrograph along the same zone (Figure 5, a), the presence of several domains tilted by 90° to each other around the *c* axis, is apparent. Each domain shows the structural features corresponding to this member of the series (see the magnification of one domain depicted in Figure 3, b). The simulated image (inset in Figure 3, b) agrees with the experimentally ascertained one for $\Delta t = 8.5$ and $\Delta f = -90$ nm. The optical Fourier transforms at the two sides of the twin plane are depicted in Figure 5 (c and d). In each domain, the modulation appears either along the [*h*0*i*4*h*]* or along the [$\bar{h}$0*i*4*h*] directions. Juxtaposition of the patterns (Figure 5, e) results in the experimental SAED shown in Figure 4 (a).

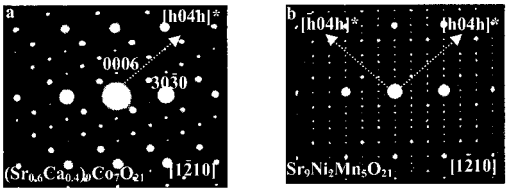

Figure 4. SAED patterns along the [1$\bar{2}$10] zone axis, corresponding to $Sr_9Ni_2Mn_5O_{21}$ (a) and $(Sr_{0.6}Ca_{0.4})_9Co_7O_{21}$ (b)

Structural Refinement

The fitting of experimental XRD patterns of the title compounds has been carried out by using as starting structural models those developed from SAED and HREM data. Thus, $Sr_{3.75}Ba_{1.25}Mn_3NiO_{12}$ consists of parallel chains made up of units of three face-sharing octahedra ($3O_h$) linked by a trigonal prism (TP), the sequence along a chain being: $-TP-3O_h-TP-3O_h-TP-3O_h-$. The structure of $Sr_9Mn_5Ni_2O_{21}$, on the other hand, is slightly more complex: the chains are made up of units of three face-sharing octahedra and units of two octahedra ($2O_h$) linked by trigonal prisms in a sequence: $-TP-3O_h-TP-2O_h-TP-3O_h-TP-2O_h-$.

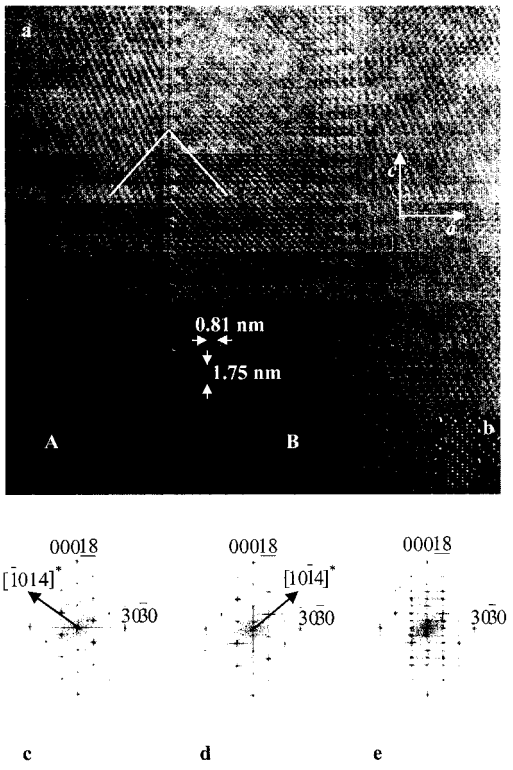

Figure 5. (a) HREM of $Sr_9Ni_2Mn_5O_{21}$ along [1$\bar{2}$10], a multitwinned microstructure can clearly be seen; (b) magnification of one of the microdomains shown in Figure 5 (a), calculated image is shown in the inset, optical Fourier transforms (FTs) corresponding to domains marked with A (c) and B (d) in Figure 5 (a); (e) FT corresponding to the juxtaposition of both A and B domains

On the basis of previous studies on similar systems,[14–17] we assume that the nickel ions are located in the prisms whereas the manganese atoms occupy the octahedra. It should be remarked that it is not possible to ascertain the actual occupation of both types of positions from XRD data. However, it was evident from the structural refinement that the atoms in the prisms are split into two positions. The atoms at the centre of the prisms are partially displaced towards the three square faces of the prisms, whereas the remaining atoms at the centres are displaced to one of the trigonal faces in some cases. This structural feature has very commonly been observed for nickel.[4,16,20]

Figure 1 (a and b) shows the result in graphic form of the fitting of the experimental X-ray diffraction pattern and the difference between observed and calculated data for $Sr_{3.75}Ba_{1.25}NiMn_3O_{12}$ and $Sr_9Ni_2Mn_5O_{21}$, respectively. The final structural parameters are collected in Tables 1 and 2, whereas Tables 3 and 4 show some selected interatomic distances. Figures 6 and 7 depict schematic representations of the structures of $Sr_{3.75}Ba_{1.25}NiMn_3O_{12}$ and $Sr_9Ni_2Mn_5O_{21}$, respectively.

As is well known, X-ray diffraction is not the best technique with which to study structural effects relating to light atoms such as oxygen in a "matrix" of metallic atoms, as is

Table 1. Final structural parameters of $(Sr_{0.75}Ba_{0.25})_5NiMn_3O_{12}$ [space group $P\bar{3}c$ (no. 165), a = 0.97114(2) nm, c = 2.03649(6) nm, V = 1.66334(7) nm^3, R_B = 0.070, R_{exp} = 0.058, R_{wp} = *0.18,* χ^2 = *10.1]*

Atom	*x/a*	*y/b*	*z/c*	*B* [Å^2]	Occupation
Sr(1)/Ba(1)	0.6786(9)	0.0064(8)	0.0500(9)	0.95(4)	0.75:0.25
Sr(2)/Ba(2)	0.3368(8)	0.0142(7)	0.1526(7)	0.95(4)	0.75:0.25
Sr(3)/Ba(3)	0.6547(7)	0	1/4	0.95(4)	0.75:0.25
Mn(1)	0	0	0	1.98(6)	1
Mn(2)	1/3	2/3	0.170(1)	1.98(6)	1
Mn(3)	1/3	2/3	0.297(2)	1.98(6)	1
Mn(4)	0	0	0.124(2)	1.98(6)	1
Mn(5)	1/3	2/3	0.420(1)	1.98(6)	1
Ni1Pc	0	0	1/4	1.44(5)	0.10(3)
Ni1Pd	−0.088(6)	−0.088(6)	1/4	1.44(5)	0.90(3)
Ni2Pc	1/3	2/3	0.059(2)	1.44(5)	0.28(4)
Ni2Pd	0.266(4)	0.600(4)	0.059(2)	1.44(5)	0.72(4)
O(1)	0.174(5)	−0.008(5)	0.054(4)	0.45(7)	1
O(2)	0.167(6)	0.666(5)	0.122(4)	0.45(7)	1
O(3)	0.516(6)	0.184(4)	0.020(3)	0.45(7)	1
O(4)	0.334(4)	0.815(6)	0.248(2)	0.45(7)	1
O(5)	0.147(5)	0.162(5)	0.178(3)	0.45(7)	1
O(6)	0.515(5)	0.346(6)	0.156(2)	0.45(7)	1

Table 2. Final structural parameters of $Sr_9Ni_2Mn_5O_{21}$ [space group $R\bar{3}c$ (no. 167), a = 0.96065(5) nm, c = 3.5836(2) nm, V = 2.8640(3) nm^3, R_B = 0.089, R_{exp} = 0.094, R_{wp} = *0.19,* χ^2 = *5.3]*

Atom	*x/a*	*y/b*	*z/c*	B (Å^2)	Occupation
Sr(1)	0.6507(7)	−0.0002(9)	0.1391(2)	0.93(6)	1
Sr(2)	0.325(1)	0	3/4	0.93(6)	1
Mn(1)	0	0	0	0.3(1)	1
Mn(2)	0	0	0.0688(4)	0.3(1)	1
Mn(3)	0	0	0.2140(5)	0.3(1)	1
Ni1Pc	0	0	0.367(4)	0.1(1)	0.22(6)
Ni1Pd	−0.064(5)	−0.064(5)	0.361(1)	0.1(1)	0.78(6)
O(1)	0.503(5)	0.165(4)	0.366(1)	0.21(7)	1
O(2)	0.828(4)	−0.015(5)	0.317(1)	0.21(7)	1
O(3)	−0.166(5)	0	3/4	0.21(7)	1
O(4)	0.504(3)	0.311(4)	0.4299(9)	0.21(7)	1

the case of our materials. However, the refinements were stable and it was possible to refine the positions of the oxygen atoms, provided that the number of refined parameters was kept not too large, which is why we used the same temperature factor for various atoms in some cases. The metal−oxygen distances in Tables 3 and 4 should therefore be regarded with some caution, although the metallic coordination (i.e., the polyhedra defined by the closest oxygen atoms around a given metal atom) is undoubtedly correct, as are the metal−metal distances.

The crystal structure of $(Sr_{0.75}Ba_{0.25})_5NiMn_3O_{12}$ is made up of one-dimensional $[Mn_{3/4}Ni_{1/4}O_3]$ chains. The space between chains is occupied by the Ba/Sr metal atoms, coordinated to oxygen atoms at distances ranging between 2.3 and 2.99 Å. There are two crystallographically different types of chains (see Figure 6), one involving −Mn(2)−Mn(3)−Mn(5)−Ni(2)− cations and the other one composed of an −Mn(4)−Mn(1)−Ni(1)− cationic sequence. The octahedral environments of Mn(1), (2) and (5) are quite regular, with average M−O distances corresponding to 2.05, 2.01 and 2.04 Å, respectively. The octahedra

Table 3. Selected interatomic distances less than 3.0 Å in $(Sr_{0.75}Ba_{0.25})_5NiMn_3O_{12}$; i and ii: generated by symmetry operations

Sr(1)/Ba(1)−O(1)	2.78(8)	Mn(1)−O(1)	2.05(2) × 6
Sr(1)/Ba(1)−O(1)^{i}	2.70(6)		
Sr(1)/Ba(1)−O(1)^{ii}	2.55(4)	Mn(2)−O(2)	1.88(2) × 3
Sr(1)/Ba(1)−O(2)	2.25(4)	Mn(2)−O(4)	2.14(2) × 3
Sr(1)/Ba(1)−O(3)	2.93(6)		
Sr(1)/Ba(1)−O(3)^{i}	2.82(6)	Mn(3)−O(4)	1.75(2) × 3
Sr(1)/Ba(1)−O(3)^{ii}	2.35(4)	Mn(3)−O(6)	1.80(2) × 3
Sr(1)/Ba(1)−O(6)	2.76(5)		
		Mn(4)−O(1)	2.25(2) × 3
Sr(2)/Ba(2)−O(1)	2.50(4)	Mn(4)−O(5)	1.87(2) × 3
Sr(2)/Ba(2)−O(2)	2.99(8)		
Sr(2)/Ba(2)−O(2)^{i}	2.96(7)	Mn(5)−O(3)	1.90(1) × 3
Sr(2)/Ba(2)−O(4)	2.73(6)	Mn(5)−O(6)	2.18(2) × 3
Sr(2)/Ba(2)−O(4)^{i}	2.66(5)		
Sr(2)/Ba(2)−O(5)	2.90(6)	Ni1Pc−O(5)	2.09(1) × 6
Sr(2)/Ba(2)−O(5)^{i}	2.75(7)		
Sr(2)/Ba(2)−O(6)	2.79(8)	Ni1Pd−O(5)	1.91(1) × 2
Sr(2)/Ba(2)−O(6)^{i}	2.67(5)	Ni1Pd−O(5)^{i}	2.00(1) × 2
		Ni1Pd−O(5)^{i,i}	2.77(2) × 2
Sr(3)/Ba(3)−O(4)	2.70(4) × 2		
Sr(3)/Ba(3)−O(4)^{i}	2.81(6) × 2	Ni2Pc−O(2)	2.06(2) × 3
Sr(3)/Ba(3)−O(5)	2.36(4) × 2	Ni2Pc−O(3)	2.17(3) × 3
Sr(3)/Ba(3)−O(6)	2.53(4) × 2		
		Ni2Pd−O(2)	1.90(4) × 2
		Ni2Pd−O(3)	2.05(1) × 2
		Ni2Pd−O(2)^{i}	2.60(3)
		Ni2Pd−O(3)^{i}	2.65(4)
Mn(1)−Mn(4)	2.53(4) × 2	Mn(3)−Mn(5)	2.50(4)
Mn(2)−Mn(3)	2.60(4)	Mn(4)−Ni1Pc	2.56(3)
Mn(2)−Ni2Pc	2.25(4)	Mn(4)−Ni2Pd	2.70(4)
Mn(2)−Ni2Pd	2.34(4)	Mn(5)−Ni2Pc	2.83(4)
		Mn(5)−Ni2Pd	2.91(4)

Table 4. Selected interatomic distances less than 3.0 Å in $Sr_9Ni_2Mn_5O_{21}$; i and ii: generated by symmetry operations

Sr(1)−O(1)	2.61(4)	Mn(1)−O(1)	1.97(4) × 6
Sr(1)−O(1)^{i}	2.82(4)		
Sr(1)−O(1)^{ii}	2.65(3)	Mn(2)−O(1)	2.05(3) × 3
Sr(1)−O(2)	2.38(4)	Mn(2)−O(4)	1.77(3) × 3
Sr(1)−O(2)^{i}	2.69(4)		
Sr(1)−O(2)^{ii}	2.80(5)	Mn(3)−O(2)	1.93(4) × 3
Sr(1)−O(3)	2.52(1)	Mn(3)−O(3)	2.05(3) × 3
Sr(1)−O(4)	3.00(3)		
Sr(1)−O(4)^{i}	2.44(4)	Ni1Pc−O(2)	2.40(5) × 3
		Ni1Pc−O(4)	1.96(5) × 3
Sr(2)−O(1)	2.46(4) × 2		
Sr(2)−O(2)	2.85(4) × 2	Ni1Pd−O(2)	2.06(6)
Sr(2)−O(3)	2.70(4) × 2	Ni1Pd−O(2)^{i}	2.13(6)
Sr(2)−O(4)	3.00(3) × 2	Ni1Pd−O(4)	1.94(5)
Sr(2)−O(4)^{i}	2.71(4) × 2	Ni1Pd−O(4)^{i}	2.04(4)
		Ni1Pd−O(2)^{i,i}	2.71(5)
		Ni1Pd−O(4)^{i,i}	2.58(5)
Mn(1)−Mn(2)	2.46(2) × 2	Mn(3)−Mn(3)	2.58(2)
Mn(2)−Ni1Pc	2.30(5)	Mn(3)−Ni1Pc	2.91(6)
Mn(2)−Ni1Pd	2.60(4)	Mn(3)−Ni1Pd	2.75(4)

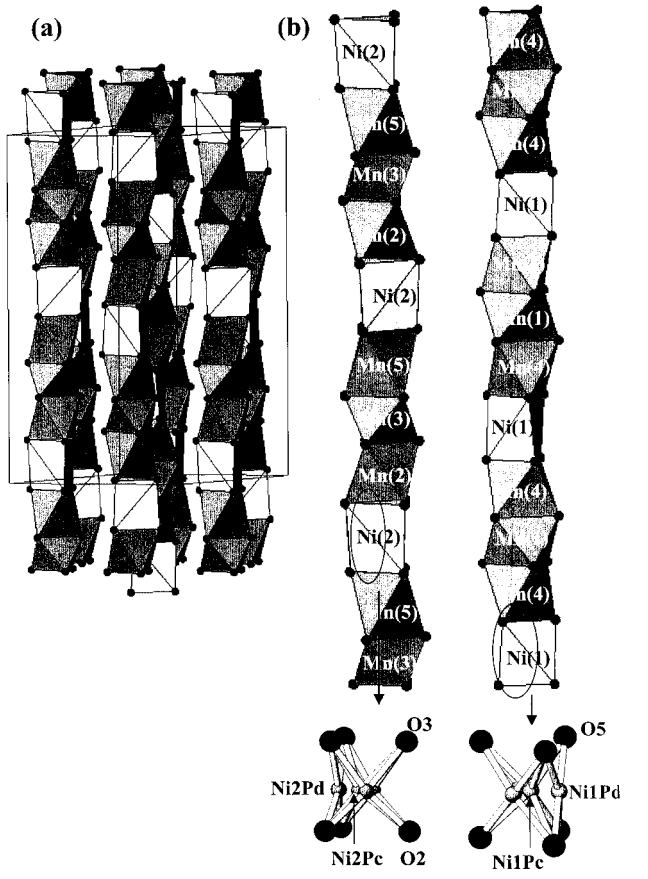

Figure 6. (a) Schematic representation of the structure of $(Sr_{0.75}Ba_{0.25})_5NiMn_3O_{12}$ (Ba/Sr atoms have been omitted for clarity); (b) the metallic sequence along the chains and the split of Ni ions in prismatic coordination are detailed

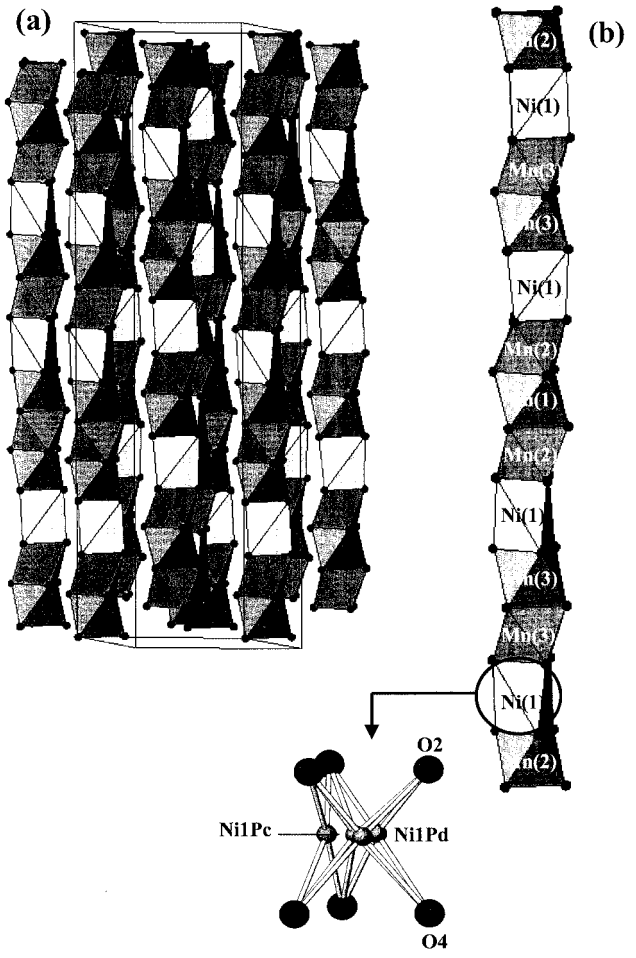

Figure 7. (a) Schematic representation of the structure of $Sr_9Ni_2Mn_5O_{21}$ (Sr atoms have been omitted for clarity); (b) the metallic sequence along the chains and the split of Ni ions in prismatic coordination are detailed

occupied by Mn(3) are less voluminous, with an average metal−oxygen distance of 1.80 Å. On the other hand, the Mn(4) atoms seem to be slightly displaced from the centres of the polyhedra, giving rise to distorted octahedra with average Mn(4)−O distance of 2.06 Å. A similar displacement of Mn has been reported in $Ba_6Mn_4ZnO_{15}$.[11] All the Mn−O distances in $(Sr_{0.75}Ba_{0.25})_5Mn_3NiO_{12}$ are similar to those previously reported in manganese-containing oxides. A particular feature of this structure is the Ni distribution in the TP sites. As can be seen in Table 1, most of the Ni cations (close to 80%) are displaced from the centres towards the square faces of the prisms. Only a small fraction (10%) of Ni(1), labelled as Ni1Pc in Tables 1 and 3, remains at the centres of the TP sites, with six equal Ni1Pc−O distances of 2.09 Å. The environments of the Ni2Pc atoms are less regular, since two different (but close) values of Ni2Pc−O distances are observed [$d_{average}$(Ni2Pc−O) = 2.11 Å]. These distances are very close to those found for Ni atoms in corresponding oxygen environments in Ca_3MnNiO_9 ($d_{average}$ = 2.145 Å)[14] and $Sr_4Ni_3O_9$ ($d_{average}$ = 2.09, 2.195 Å).[4] The remaining Ni1 and Ni2 (referred to as Ni1Pd and Ni2Pd in Table 1) are in square-planar coordination with average M−O distances of 1.95 and 1.97 Å, respectively; these values are also in agreement with Ni^{II}−O distances measured in comparable oxides with similar displacements of the Ni atoms, as in $Sr_4Ni_3O_9$ ($d_{average}$= 1.95, 2.07 Å) or $Sr_4NiMn_2O_9$ ($d_{average}$ = 2.02, 1.99 Å).[4,16] With regard to the M−M distances, the Mn−Mn ones range from 2.50 to 2.60 Å, characteristic of Mn^{IV}−Mn^{IV} in face-sharing octahedra. A similar value is obtained for the Ni1Pc−Mn distance (2.56 Å), but Ni2Pc is slightly displaced towards one of the triangular faces of the TP, giving rise to two very different distances to the neighbour Mn metal atoms. This feature has also been observed in $Sr_4NiMn_2O_9$.[16]

The structure of $Sr_9Ni_2Mn_5O_{21}$ also contains face-sharing [Mn/Ni]-polyhedra chains linked together by Sr−O bonds. The Sr cations are in nine- or tenfold coordination, at distances ranging from 2.38 to 3.00 Å. $Mn(1)O_6$ and $Mn(3)O_6$ define fairly regular octahedra, whereas Mn(2) is located in a distorted octahedron. All the Mn−O and all the Mn−Mn distances are consistent with previously reported bond lengths in comparable manganese oxides. With respect to the Ni environment, about 80% of the Ni atoms once again adopt square-like coordinations [$d_{average}$(NiPd−O) = 2.04 Å]. The remaining Ni atoms, lo-

cated in trigonal-prismatic coordinations, are each displaced from the centre towards a triangular face of the TP, giving rise to three short (1.96 Å) and three long (2.4 Å) NiPc−O distances. This displacement gives rise to a short Mn(2)−NiPc distance (2.30 Å), close to that found in $Sr_4NiMn_2O_9$ (2.32 Å).[16]

Conclusions

The structural refinement shows that the two new one-dimensional Mn/Ni oxides present the general structural features corresponding to the ($\alpha = 3$, $\beta = 2$) and the ($\alpha = 2$, $\beta = 1$) members of the $(A_3A'BO_6)_\alpha(A_3B_3O_9)_\beta$ series for the $(Sr_{0.75}Ba_{0.25})_5NiMn_3O_{12}$ and $Sr_9Ni_2Mn_5O_{12}$ compositions, respectively. The particular characteristic of each structure is the displacement of most of the Ni atoms from the centres of the trigonal prisms toward the square faces. On the other hand, both materials present twinned microstructures. The presence of twinning in this type of oxides is usually observed when some cationic disorder exists through the polyhedra chains. In this sense, when metal cations of different chemical natures are randomly distributed in the Oh and the TP sites, twinned one-dimensional oxides result. In the samples studied, $Sr_9Mn_5Ni_2O_{21}$ and $Sr_{3.75}Ba_{1.25}NiO_{12}Mn_3$, there is no disorder relative to the cationic distribution in the two different oxygen environments since Mn is located in the octahedra whereas Ni is occupying the trigonal prisms. However, the particular arrangement of the Ni atoms in the TP sites could induces a certain disorder at the Ni positions, most probably the origin of the multi-twinning in the crystals.

Experimental Section

Polycrystalline $Sr_{3.75}Ba_{1.25}NiMn_3O_{12}$ and $Sr_9Ni_2Mn_5O_{21}$ were synthesised by the ceramic procedure by heating stoichiometric amounts of ACO_3 (A = Sr, Ba) (Aldrich, 99.9+%), $MnCO_3$ (Aldrich, 99.9+%) and NiO (Aldrich, 99.99%) in air. The former was treated at 1200 °C for 3 days and the latter at 1050 °C for 6 days with intermediate grinding. In both cases the products were quenched to room temperature.

The average cationic composition was determined by Inductive Coupled Plasma (ICP) while the local composition in every crystal was established by X-ray Energy Dispersive Spectroscopy (EDS). A JEOL 2000 FX electron microscope equipped with an OXFORD ISIS 300-analyser system was employed for this purpose.

Powder X-ray diffraction (XRD) patterns were collected by use of Cu-K_α radiation at room temperature with a PHILIPS X'PERT diffractometer equipped with a graphite monochromator. The diffraction data were analysed by the Rietveld[21] method, by use of the Fullproff program.[22]

Selected Area Electron Diffraction (SAED) was carried out with a JEOL 2000FX electron microscope fitted with a double-tilting goniometer stage (±45°). High-Resolution Electron Microscopy (HREM) was performed with a JEOL 4000EX electron microscope fitted with a double-tilting goniometer stage (±25°). Simulated HREM images were calculated by the multislice method with the aid of the MacTempas software package.

Acknowledgments

Financial support through research project MAT2001-1440 (CICYT, Spain) is acknowledged.

[1] J. J. Lander, *Acta Crystallogr.* **1951**, *4*, 148.
[2] G. Bergerhoff, O. Schmitz-Dumont, *Z. Anorg. Allg. Chem.* **1956**, *10*, 284.
[3] K. Boulahya, M. Parras, J. M. González-Calbet, *Chem. Mater.* **2000**, *12*, 25.
[4] F. Abraham, S. Minaud, C. Renard, *J. Mater. Chem.* **1994**, *4*, 1763.
[5] J. A. Campá, E. Gutiérrez-Puebla, M. A. Monge, I. Rasines, C. Rúiz-Valero, *J. Solid State Chem.* **1994**, *108*, 230.
[6] K. Boulahya, M. Parras, J. M. González-Calbet, *J. Solid State Chem.* **1999**, *145*, 116−127.
[7] W. T. A. Harrison, S. L. Hegwood, A. J. Jacobson, *J. Chem. Soc., Chem. Commun.* **1995**, 1953.
[8] K. Boulahya, M. Parras, J. M. González-Calbet, *J. Solid State Chem.* **1999**, *142*, 419−427.
[9] K. Boulahya, M. Parras, J. M. González-Calbet, J. L. Martínez, *Chem. Mater.* **2002**, *14*, 4006.
[10] L. Katz, R. Ward, *Inorg. Chem.* **1964**, *3*, 205−211.
[11] E. J. Cussen, J. F. Vente, P. D. Battle, *J. Am. Chem. Soc.* **1999**, *121*, 3958−3967.
[12] M. Hernando, K. Boulahya, M. Parras, J. M. González-Calbet, *Eur. J. Inorg. Chem.* **2002**, *12*, 3190−3196.
[13] V. G. Zubkov, G. V. Bazuev, A. P. Tyutyunnik, I. F. Berger, *J. Solid State Chem.* **2001**, *160*, 293−301.
[14] G. V. Bazuev, V. G. Zubkov, I. F. Berger, T. I. Arbuzova, *Solid State Science* **1999**, *1*, 365−372.
[15] S. Kawasaki, M. Takano, *J. Solid State Chem.* **1999**, *145*, 302−308.
[16] A. El Abed, E. Gaudin, S. Lemaux, J. Darriet, *Solid State Sciences* **2001**, *3*, 887−897.
[17] A. El Abed, E. Gaudin, J. Darriet, M.-H. Whangbo, *J. Solid State Chem.* **2002**, *163*, 513−518.
[18] J. L. Hodeau, H. Y. Tu, P. Bordet, T. Fournier, P. Strobel, M. Marezio, *Acta Crystallogr., Sect. B* **1992**, *48*, 1−11.
[19] P. D. Battle, G. R. Blake, J. Sloan, J. F. Vente, *J. Solid State Chem.* **1998**, *136*, 103−114.
[20] M. Evain, F. Boucher, O. Gourdon, V. Petricek, M. Dusek, P. Bezdicka, *Chem. Mater.* **1998**, *10*, 3068−3076.
[21] H. M. Rietveld, *J. Appl. Crystallogr.* **1969**, *2*, 65−71.
[22] J. Rodríguez-Carvajal, *Physica B.* **1993**, *192*, 55−69.

Received January 13, 2003

